DOI: 10.22146/jnteti.v14i1.15001

Optical Flow Performance in the SUAV Flight Speed Estimation Using Farneback Method

Aziz Fathurrahman[1], Ony Arifianto[1], Yazdi Ibrahim Jenie[1], Hari Muhammad[1]

[1] Faculty of Mechanical and Aerospace Engineering, Institut Teknologi Bandung, Bandung, Jawa Barat 40132, Indonesia

[Received: 21 August 2024, Revised: 11 August 2024, Accepted: 15 January 2025]
Corresponding Author: Aziz Fathurrahman (email: 33621003@mahasiswa.itb.ac.id)

ABSTRACT — This paper evaluates the performance of the Farneback optical flow method for estimating the flight speed of a small unmanned aerial vehicle (SUAV) in a simulated 3D World MATLAB-Unreal Engine environment. Optical flow offers a promising solution for velocity estimation, which is crucial for autonomous navigation. A downward-facing monocular camera model was simulated on an SUAV during steady state, straight flight at 100 m altitude and 25 m/s airspeed. Three simulated flight scenes—forest, city block, and water—representing poor, moderate, and rich textures were used to assess the method's performance. Results demonstrate that using the median estimate of the optical flow field yields accurate velocity estimations in moderate to rich texture scenes. Over the city block and forest scenes, mean velocity estimation accuracy was 0.6 m/s (σ = 0.2 m/s) and 0.3 m/s (σ = 0.4 m/s), respectively. The impact of camera tilt angle and altitude variations on estimation accuracy was also investigated. Both factors introduced bias, with accuracy decreasing to 1.7 m/s (σ = 0.2 m/s) and 1.9 m/s (σ = 0.2 m/s) for +10° and -10° camera tilt, respectively. Similarly, altitude differences of +10m and -10m resulted in reduced accuracy of 1.9 m/s (σ = 0.2 m/s) and 4.3 m/s (σ = 0.1 m/s), respectively. This study demonstrates the potential of the Farneback method for determining flight speed under steady, straight flight conditions with acceptable accuracy.

KEYWORDS — Flight Speed Estimation, Small UAV, Optical Flow, Performance Assessment.

I. INTRODUCTION

Interest in the unmanned aerial vehicle (UAV), or drone, has increased over the last decade due to its versatile capability to conduct several tasks that can benefit from carrying out payloads in the air. The UAV has demonstrated its useful application in military and civilian domains, such as for aerial surveillance [1], parcel delivery [2], traffic monitoring [3], search and rescue operations [4], precision agriculture [5], and remote sensing [6]. Especially for a small UAV (SUAV) [7], its application domain has expanded significantly owing to its affordable price and ease of deployment compared to larger UAVs. Hence, there has been a notable surge in research interest focused on the SUAV aimed at enhancing its functionality through the pursuit of full autonomy [8].

Nevertheless, autonomous SUAVs require accurate and robust navigation systems to ensure the safe completion of their mission while avoiding harm to the SUAVs and their surroundings. The main problem in SUAV navigation focuses on improving Global Navigation Satellite Systems (GNSS) to have accurate navigation output when the source of data is unavailable due to unexpected outages or problems derived from intentional attacks in GNSS-denied environments, such as signal interference (jamming) or fake signal generation (spoofing). Therefore, an approach based on sensor fusion is essential as a resort to the fundamental equation of navigation and the characterization of the errors committed by each sensor [9], [10]. In order to establish a navigation system that is more accurate and robust, the sensor fusion approach integrates more information from multiple sensors. Sensor fusion allows different kinds of sensors to be utilized for navigation. Conventional sensor for SUAV navigation commonly consists of inertial measurement unit (IMU) and GNSS. Although IMU has relatively fast sampling rate, its accuracy is declining over time because of inherent bias and noise [11]. Meanwhile, GNSS accuracy can be considered constant, but it relies heavily on the satellite external signal that may be degraded, denied, or even spoofed in an unexpected condition [12]. The alternative complementary sensors for IMU and GNSS are altitude barometer, magnetic compass, Wi-Fi, Bluetooth, radio-frequency identification, ultra-wideband, ultrasonic, light detection and ranging (LiDAR), 5G, and camera [11]. Despite many alternatives as an aiding sensor for IMU and GNSS, this paper focuses on an onboard camera because it does not rely on external signal source and has great a potential for further development. It has been found out that flying insects use their vision for navigation [13]. Therefore, camera or vision-based navigation is a natural solution for flying vehicles. Many algorithms for navigation based on sensor have been developed, this paper focuses on optical flow as researchers recently focused on indoor navigation, but only few studying optical flow for outdoor navigation [8].

The optical flow estimation for SUAV navigation is an ongoing research field. The earliest recognized works on the optical flow estimation for aerial vehicles are attributed to Grindley in 1942, Calvert in 1947, and Gibson in 1950, focusing on the importance of pilot visual cues to control aircraft during landing [14]–[16]. Furthermore, numerous researchers have discovered that optical flow estimation to aid control of motion during landing is already utilized in the expansion rate of the image to infer time to contact the surface. This fact encourages more studies on utilizing optical flow estimation for the control and navigation of vehicles, especially SUAVs.

Optical flow estimation for various SUAV navigation subtasks have been studied based on image sensors only or fused with other sensors, including for distance estimation [17], altitude hold and obstacle avoidance [18], velocity and height estimation [19], and vertical landing [20]. This research

focused on flight speed estimation at outdoor flight scene, as optical flow can be a good candidate for improving IMU flight speed estimation to reduce estimation error due to IMU bias and noise. Estimated flight speed was then used for flight path reconstruction of the SUAV as part of its navigation.

Prior research conducted a quantitative assessment of the optical flow estimation accuracy for flight speed estimation at outdoor flight scenes [13]. At high speeds, motion blur can severely degrade the accuracy of optical flow estimation. Specialized algorithms that can cope with blur or alternative sensing modalities are needed for high-speed UAV applications. Prior research has shown that Farneback method is more promising method to estimate the optical flow than Lucas-Kanade and Horn-Schunk methods [21]. However, to the best of the authors' knowledge, there is currently no research examining the performance of the Farneback method in SUAV applications. Hence, this research aimed to examine the capability of the Farneback optical flow method in determining the flight speed of SUAVs for outdoor navigation using numerical simulation. With the advancement of computation technologies, numerical simulation can now offer various flight scenes to test optical flow accuracy. The results obtained from optical flow estimation are compared with analytical results (as true value) for a steady straight flight condition.

This paper focuses on assessing the performance of an optical flow approach for determining the flight speed of SUAVs for outdoor navigation. Several steps were taken. First, an SUAV performing a steady straight flight from point A to point B, as an example of a flight phase in a cargo drone mission, was modeled using the kinematics equation. In this research, a fixed-wing SUAV with a wingspan of 2 m and a maximum takeoff weight (MTOW) of 18 kg was utilized. Next, the optical flow estimation was modeled based on the recorded videos. Then, a 3D virtual world was utilized for a simulation with three scenes: city block, forest, and water. Last, different factors that could affect optical flow performance were observed and compared, including altitude and camera tilting angle to the navigation parameters, especially velocity, and potion of the SUAVs in the local horizon frame of reference.

II. OPTICAL FLOW-BASED NAVIGATION OF THE SUAV

The optical flow is defined as the apparent motion of the image intensity or brightness intensity due to the 2D projection of the relative 3D motion of scene points onto the camera (as an image sensor). In an ideal condition, it corresponds to the velocity field in the image plane (or visual displacement of image points) obtained from the 2D projection of the speed of the moving object in the 3D space. This movement in image plane can be used to infer the movement of the camera relative to a real-world object.

A. DOWNWARD-LOOKING CAMERA SETUP ON SUAV

Downward-looking camera setup (Figure 1) is regarded as the most common setup in numerous recent SUAV navigation studies. This camera setup simplifies the problem of estimating the SUAV velocity since the camera axes (x_c, y_c, and z_c) are aligned with the SUAV body axes (x_b, y_b, and z_b). Therefore, the movement of the camera represents the movement of the SUAVs in its body axes. The downward-looking camera captures or samples an image every sampling time; in this study, 30 Hz was selected as typical sampling rate of monocular

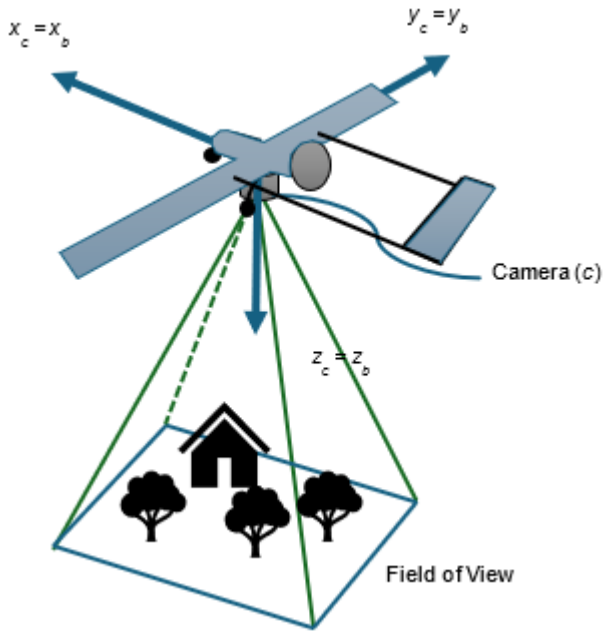

Figure 1. Camera setup represented by camera axes (c) and SUAV orientation represented by body axes (b), z_c is camera lens direction.

camera installed on the SUAV. Images captured by the camera then were used to estimate the optical flow.

B. OPTICAL FLOW GENERATED BY THE CAMERA MOTION

Based on the definition of the optical flow mentioned at the beginning of Section 2, the optical flow between two consecutive images can be calculated from the movement of pixels with the same brightness or intensity value from the prior image frame to the next image frame (two consecutive frames), as illustrated in Figure 2. Conservation of intensity of a pixel between two consecutive image frames is modeled using (1) [22]:

$$I(x_c, y_c, t) = I(x_c + dx_c, y_c + dy_c, t + dt) \quad (1)$$

where $I(x_c, y_c, t)$ is the intensity of a pixel at coordinate (x_c, y_c) in image frame at time prior time (t) and $I(x_c + dx_c, y_c + dy_c, t + dt)$ is the intensity of a pixel at coordinate $(x_c + dx_c, y_c + dy_c)$ and posterior time $(t + dt)$.

Based on the conservation of intensity, a well-known optical flow or gradient constraint [23] can be derived,

$$OF_x\left(\frac{\partial I}{\partial x_c}\right) + OF_y\left(\frac{\partial I}{\partial y_c}\right) + \left(\frac{\partial I}{\partial t}\right) = 0 \quad (2)$$

where OF_x and OF_y are the optical flow components in the coordinate x_c and y_c of a point in the image frame.

In an actual flight, SUAVs can move in six degrees of freedom (DOF), consisting of 3DOF translational motion (u, v, and w) and 3DOF rotational motion (p, q, and r) in body axes. Therefore, the relationship between the optical flow of a point in an image plane and SUAV motion is commonly modeled as in (3).

$$\begin{pmatrix} OF_x \\ OF_y \end{pmatrix} = T_{OF} + R_{OF} \quad (3)$$

with the translational part (T_{OF}) being

$$T_{OF} = \frac{1}{z_c}\begin{bmatrix} -f & 0 & x_c \\ 0 & -f & y_c \end{bmatrix}\begin{pmatrix} u \\ v \\ w \end{pmatrix} \quad (4)$$

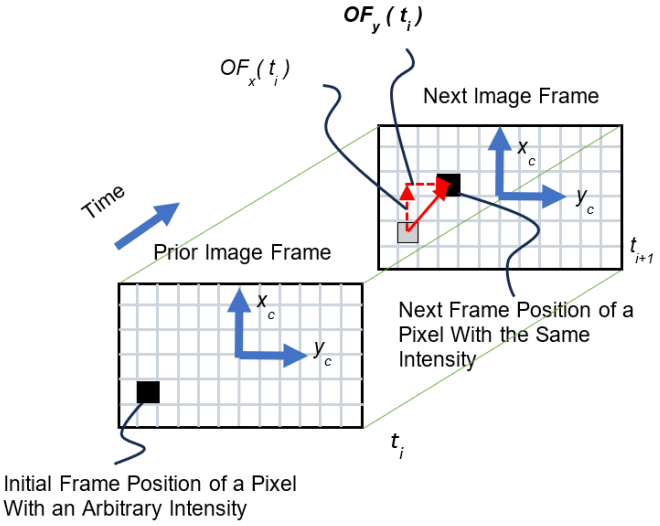

Figure 2. Optical flow between two consecutive frames.

and the rotational part (R_{OF}) being

$$R_{OF} = \begin{bmatrix} \frac{x_c y_c}{f} & -\left(f + \frac{x_c^2}{f}\right) & y_c \\ \left(f + \frac{y_c^2}{f}\right) & -\frac{x_c y_c}{f} & -x_c \end{bmatrix} \begin{pmatrix} p \\ q \\ r \end{pmatrix} \quad (5)$$

where OF_x and OF_y are the optical flow components in the coordinate x and y of a point in the image frame. Meanwhile, $(u \quad v \quad w)^T$ and $(p \quad q \quad r)^T$ are the translational velocity and rotational rate in the SUAV body axes, and f is the focal length of the camera model. For a steady straight flight condition (no rotation and constant altitude) with a downward-looking camera setup, (3) can be simplified into (6).

$$\begin{pmatrix} OF_x \\ OF_y \end{pmatrix} = \frac{1}{z_c} \begin{bmatrix} -f & 0 \\ 0 & -f \end{bmatrix} \begin{pmatrix} u \\ v \end{pmatrix} \quad (6)$$

where R_{OF} is omitted and $w = 0$.

The downward-looking camera motion, along with the SUAV motion, results in the optical flow field of the image plane. A 720 × 1280 pixel, or commonly called 720p image quality, was used. From the resulting optical flow field (720 × 1280 pixels), median values were used to represent the global optical flow. Then, from the global optical flow (OF_x and OF_y), (4) was used to obtain u and v. This research considered only the SUAV motion in x_b and y_b or velocity components u and v, while other states remained constant. In several research, optical flow is commonly fused with other sensors, such as a gyroscope and height or depth sensor, to supply information on the rotational movement (p, q, and r) and the change of altitude ($-\Delta z_c$). Hence, one of the limitations of optical flow cameras for SUAV navigation is the limited information up to only 2DOF of motion and the requirement for additional information (sensors) to estimate the SUAV motion in 6DOF completely.

For a steady straight flight case, a single monocular camera was used to estimate the velocity (u and v) of the SUAV using the optical flow technique. Three virtual flight scenes (city block, forest, and river) were selected to simulate different levels of texture richness from an actual flight scene that would affect the estimation of the technique's accuracy. In addition, the effect of camera tilt angle and altitude on the accuracy of the technique was demonstrated through simulations.

III. MATHEMATICAL MODEL OF SUAV NAVIGATION BASED ON OPTICAL FLOW

Figure 3 illustrates how SUAV motion was simulated and how the velocity of the SUAV in North-East-Down (NED) axes was estimated. To simulate the motion of the SUAV, well-known kinematics equations and navigation equations of an aircraft were applied. The SUAV motion was visualized in 3D virtual flight scenes. A downward-looking camera model was combined with the SUAV model to capture video during flight, representing the single monocular camera system installed on the SUAV.

True position and attitude of the SUAV are required to generate a proper virtual world flight scene for the camera to capture. Therefore, the true position and attitude of the SUAV were inputted into the virtual world flight scene model. The on-board camera model would send a recorded video for the optical flow estimation. The optical flow estimation generated dense optical flow between two consecutive frames obtained from the recorded video. Therefore, the global optical flow must be determined to represent the SUAV's motion. The global optical flow is a single optical flow value for the whole image of each frame in the recorded video.

The global optical flow can be represented by the mean or median of the dense optical flow values as in (7). Thus, mean and median values of the dense optical flow were compared to investigate which more accurately represents the camera's motion in the real world.

$$\begin{aligned} \overrightarrow{OF}_{SUAV-mean} &= mean\left(\overrightarrow{OF_1}, \overrightarrow{OF_2}, \overrightarrow{OF_3}, \ldots, \overrightarrow{OF_N}\right) \\ \overrightarrow{OF}_{SUAV-median} &= median\left(\overrightarrow{OF_1}, \overrightarrow{OF_2}, \overrightarrow{OF_3}, \ldots, \overrightarrow{OF_N}\right) \end{aligned} \quad (7)$$

where $\overrightarrow{OF}_{SUAV-mean}$ is the global optical flow vector obtained from the mean value of the optical flow field consisting of x and y component, $\overrightarrow{OF}_{SUAV-median}$ is the global optical flow obtained from the median value of the optical flow field consisting of x and y components, and $\overrightarrow{OF_1}, \overrightarrow{OF_2}, \overrightarrow{OF_3}, \ldots, \overrightarrow{OF_N}$ is the optical flow vector of each pixel, from pixel 1 until pixel N, where N is 720 × 1280.

A. SUAV MODEL

Based on a well-known kinematics equation (8) and navigations equations of an aircraft (9), the SUAV is modeled as a rigid-body aircraft with constant mass.

$$\begin{aligned} \dot{u} &= -qw + rv - g\sin\theta + a_{xb} \\ \dot{v} &= -ru + pw + g\cos\theta\sin\varphi + a_{yb} \\ \dot{w} &= -pv + qu + g\cos\theta\cos\varphi + a_{zb} \\ \dot{\varphi} &= p + q\sin\varphi\tan\theta + r\cos\varphi\tan\theta \\ \dot{\theta} &= q\cos\varphi - r\sin\varphi \\ \dot{\psi} &= q\sin\varphi\sec\theta + r\cos\varphi\sec\theta \end{aligned} \quad (8)$$

where $\dot{u}$, $\dot{v}$, and $\dot{w}$ are time-derivative of u, v, and w respectively; g is gravity acceleration at altitude 100 m that modeled to be 9.81 m/s^2; φ, θ, and ψ are attitude or orientation angle between body axes and NED axes that all modelled to be zero.

All forces and moments work on the SUAV at its center of gravity. Therefore, the inputs of the model are proper acceleration (a_{xb}, a_{yb}, and a_{zb}) in body axes and body rotation rate (p, q, and r) are modeled to be zero. By using the

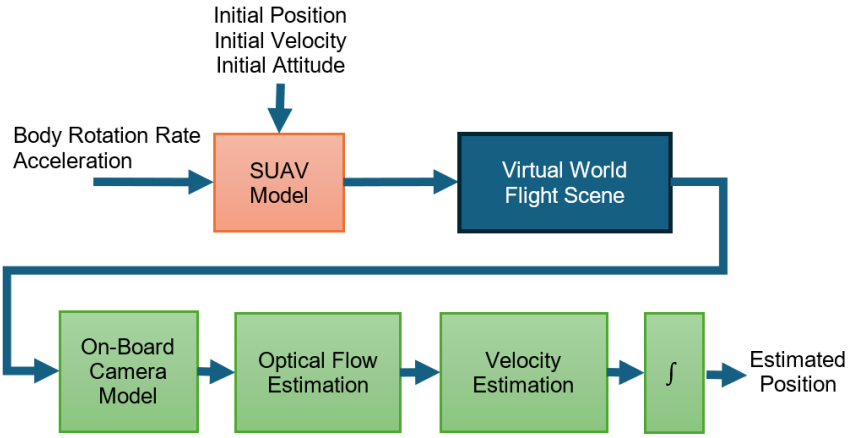

Figure 3. Simulation and estimation schematic diagram.

kinematics equation, velocity in body axes and attitude of the SUAV can be obtained.

Then, velocity in body axes and attitude of the SUAV are used to obtain velocity and position in 2D NED axes using the navigation equations for North and East velocity only while disregarding the Down velocity.

$$\begin{aligned} V_N &= u\cos\psi\cos\theta \\ &+ v\,(\cos\psi\sin\theta\sin\varphi - \sin\psi\cos\varphi) \\ &+ w\,(\cos\psi\sin\theta\cos\varphi + \sin\psi\sin\varphi) \\ V_E &= u\sin\psi\cos\theta \\ &+ v\,(\sin\psi\sin\theta\sin\varphi + \cos\psi\cos\varphi) \\ &+ w\,(\sin\psi\sin\theta\cos\varphi - \cos\psi\sin\varphi) \end{aligned} \tag{9}$$

where V_N and V_E are the velocity component in North and Down direction, respectively. Positions in North-East plane were obtained by numerically integrating the velocity components.

In this research, a steady straight flight condition was selected for the simulation. As outlined in Section II.B, the optical flow is capable of distinctly sensing up to 2DOF motion. Consequently, under the steady straight flight condition, optical flow can be utilized to estimate the velocity and position of the SUAV model because the SUAV is only moving in the x-y plane (North-East in NED axes). The steady straight flight condition is represented by (10).

$$\begin{pmatrix} u \\ v \\ w \end{pmatrix} = \begin{pmatrix} 25 \\ 0 \\ 0 \end{pmatrix} m/s \qquad \begin{pmatrix} \varphi \\ \theta \\ \psi \end{pmatrix} = \begin{pmatrix} 0 \\ 0 \\ 0 \end{pmatrix} deg \tag{10}$$

Equation (10) represents the condition where translational velocity and attitude are both constant. Therefore, there is no true acceleration and rotation rate sensed by the sensor. Attitude of the SUAV in (10) indicates that body and NED axes are aligned. Thus, the velocity component in body and NED axes are equal. As a reference, true value was computed analytically for 10 s simulation and 25 m/s velocity, the SUAV translated 250 m to North from its initial position.

B. VIRTUAL WORLD FLIGHT SCENES

The virtual world flight scenes were generated using an Unreal Engine integrated with MATLAB Simulink. The Unreal Engine was employed to visualize the motion of the SUAV and the on-board camera models. The Unreal Engine is a game engine developed by Epic Games, allowing users to render 3D virtual world for the flight scenes. Three flight scenes were utilized, including US city block scene provided by MATLAB, forest scene, and water scene (Figure 4).

C. ON-BOARD CAMERA MODEL

The Simulink provided simulation 3D camera was utilized to record the image captured by the on-board camera while the SUAV was flying. The simulation 3D camera model allows users to define the position and orientation of the camera relative to the vehicle (SUAV). The output of the simulation 3D camera model is a recorded video. After the simulation was completed, the recorded video was then analyzed using the optical flow estimation technique.

D. OPTICAL FLOW ESTIMATION

Using the recorded video, the optical flow between each two consecutive frames (two frames motion) in the video, from the start until the end of the simulation, was estimated using the Farneback calculation. The Farneback calculation enhances the Lucas-Kanade method by applying pyramid coarse-to-fine estimation process [23]. Farneback algorithms can accommodate faster optical flow (> 1 pixel/frame); it is required because at an altitude of 200 m above the ground for the SUAV case, pixel velocity can surpass 1 pixel/frame for the optical flow to work. The image pyramid created by the Farneback algorithm has progressively lower resolution levels for each level than the preceding level. Beginning at the lowest resolution, the algorithm can track the points at several levels. The algorithm can accommodate a greater number of point displacements between frames by increasing the number of pyramid layers. Optical flow tracking is carried out at the lowest resolution level until convergence. Point locations identified at one level are used as reference points for subsequent levels. With every stage, the program improves tracking in this manner. The algorithm can manage huge pixel motions due to pyramid decomposition, which can be larger than the neighborhood size.

This research utilized the MATLAB function of Farneback optical flow estimation. The performance of the Farneback algorithm depends on the algorithm's properties. These properties consist of the number of pyramid layers (NumPyramidLevels), image downsampling scale (PyramidScale), number of search iterations per pyramid level (NumIterations), size of the pixel neighborhood

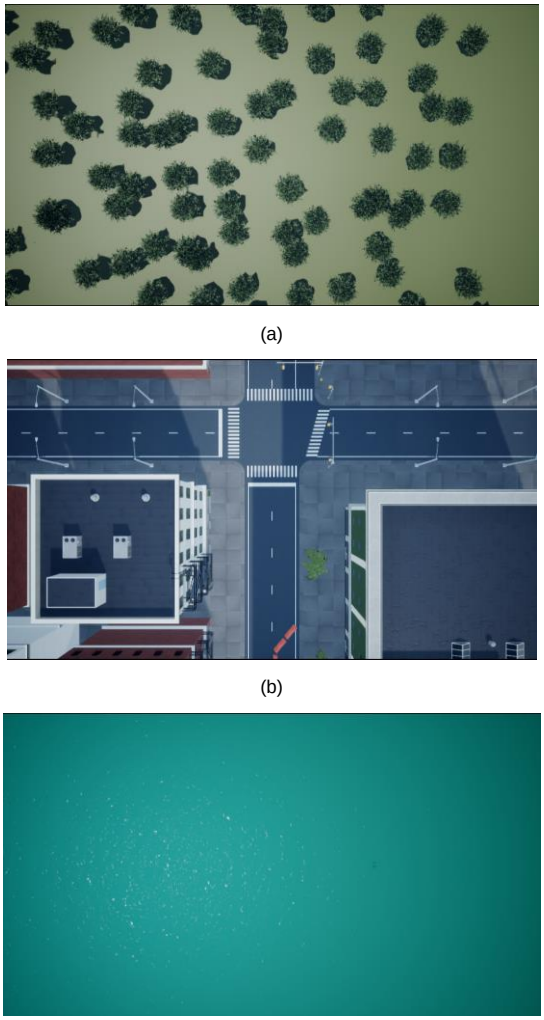

(a)

(b)

(c)

Figure 4. Virtual world flight scenes, (a) forest scene represents rich texture scene, (b) city-block scene represents moderate texture scene, and (c) water scene represents poor texture scene.

(NeighborhoodSize), and averaging filter size (FilterSize). Heuristically, based on default value provided by MATLAB, selected properties includrd NumPyramidLevels = 3, PyramidScale = 0.5, NumIterations = 3, NeighborhoodSize = 5, and esFilterSize = 60. Default property values were used except for the FilterSize, which was increased four times from its default value of 15. Increasing the filter size enhances the robustness of the algorithm to image noise. The larger the filter size, the greater the algorithm handles image noise and fast motion detection, making it more robust. In this case, the filter size needed to be increased to accommodate fast optical flow due to the flight speed of the SUAV.

E. VELOCITY AND POSITION ESTIMATION

Equation (6) was used to estimate the SUAV's velocity based on global optical flow value at steady straight flight. From the value of global optical flow, arranging (6) and substituting the z-distance of a point (z_c) with altitude (h) could estimate the u and v of the SUAV.

$$\begin{pmatrix} u \\ v \end{pmatrix} = \frac{1}{f}\begin{bmatrix} -h & 0 \\ 0 & -h \end{bmatrix}\begin{pmatrix} OF_x \\ OF_y \end{pmatrix} \quad (11)$$

where OF_x and OF_y are global optical flow obtained from mean or median value of optical flow field in pixel/s, h in m, and f in pixel.

TABLE I
TESTING SCENARIO

No	Testing Scenario	Objective	Variation
1	Different flight scenes	To get insight into the effect of texture richness in recorded videos to the accuracy of flight speed estimation.	Forest scene, city-block scene, and water scene.
2	Different camera tilting angles	To examine the effect of the camera tilting angle to the accuracy of flight speed estimation.	-30 deg, -20 deg, -10 deg, 10 deg, 20 deg, and 30-deg camera tilt angle.
3	Different altitude	To observe the effect of slight change on the flight altitude to the accuracy of the flight speed estimation.	-30 m, -20 m, -10 m, 10 m, 20 m, and 30 m altitude difference from the reference (100 m).

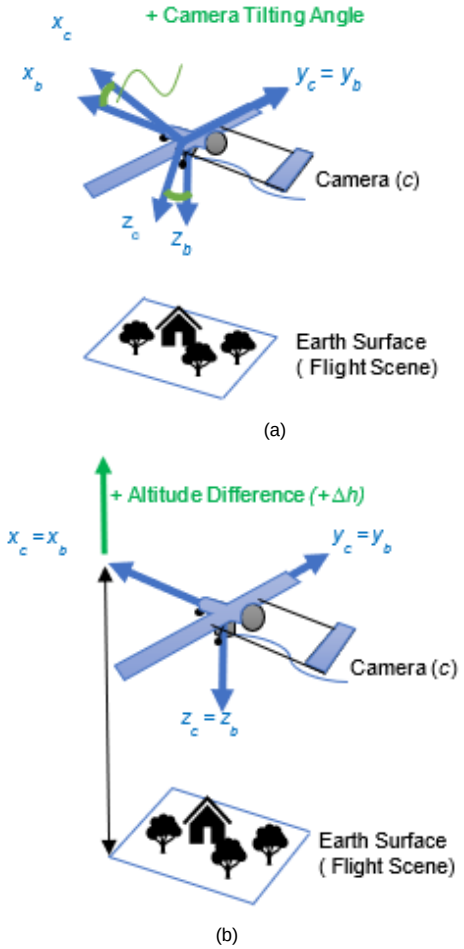

Figure 5. Testing scenario (a) different camera tilting angle and (b) different altitude. Index b indicates body-axes of the SUAV and Index c indicates camera-axes.

In this research, only a steady straight flight condition was considered. Therefore, u and v could be used to estimate velocity component in north and east direction of NED axes, while the velocity component in down direction was assumed to be zero. Position estimation for each timestep was obtained by integrating (12).

$$\begin{pmatrix} V_N \\ V_E \\ V_D \end{pmatrix} = \begin{pmatrix} u \\ v \\ 0 \end{pmatrix} \quad (12)$$

IV. SIMULATION RESULTS

The reference simulation data (true values) for the velocity and position of the SUAV were generated using (8). The estimation method was tested by conducting simulations for three different cases of stable straight flight, as detailed in Table I and in Figure 5.

A. DIFFERENT FLIGHT SCENES: FOREST, CITY BLOCK, AND RIVER

Three different flight scenes were utilized for the first case of simulation to demonstrate how texture richness of the flight scene affected the accuracy of optical flow estimates. Quantitatively, areas with little texture or uniform regions (such as water scene) lack distinctive features that are necessary for accurately tracking motion. Each scene represents different levels of texture richness: the forest for rich textures, the city block for moderate textures, and the river for poor textures. Figure 6 illustrates how the optical flow (vectors) is distributed in each of the image frames while the SUAV is moving above the scenes.

For the forest scene, shown in Figure 6(a), the optical flow is uniformly distributed due to the richness of the texture of all the trees in the scene. In the city block scene, as demonstrated in Figure 6(b), the optical flow distribution is similar with the distribution in the forest scene; therefore, the mean and median values of the distributions must be observed to see if both results are really the same. For the water scene, shown in Figure 6(c), the optical flow only appears due to the motion of sunlight reflection on the water surface. The magnitude of the optical flow was smaller compared to the optical flow in the forest and city block scene.

Figure 7 shows the time history of mean and median values of the optical flow for each flight scene. As can be seen in Figure 7, the true (reference) values for OF_x and OF_y are shown by the black color line. The closest values to the reference value are the median of optical flow in forest and city-block scenes, which are shown by the solid red and the solid green lines. The median for water scene OF_x is zero due to the poor texture of the image, even though there are sunlight reflections presented in the image. The mean values of OF_x for all scenes do not correctly represents the motion of SUAV because the distribution of optical flow is not a uniform region. The distribution also contains noise that distorts the mean value from the true value. Therefore, in this case the median value can estimate the true value better compared to the mean value.

Figure 8 shows the time history of the estimated value of the SUAV velocity in NED axes. As modeled by (9), the value of body axes and NED velocity components were identical during the steady straight flight analyzed in this study. The value of velocity components in x and y axis were directly obtained from the product of optical flow and a constant $(-h/f)$. As can be seen in Figure 8, the estimated velocity obtained from median value of optical flow in forest and city block scene are close to true value, especially for V_N.

Table II shows the mean and standard deviation of the error in estimated velocity (V_N and V_E) for each scene and the method of calculating global optical flow. The estimated velocity was subtracted with true values, which were 25 m/s for V_N and 0 m/s for V_E, to calculate the error of velocity estimation. The forest

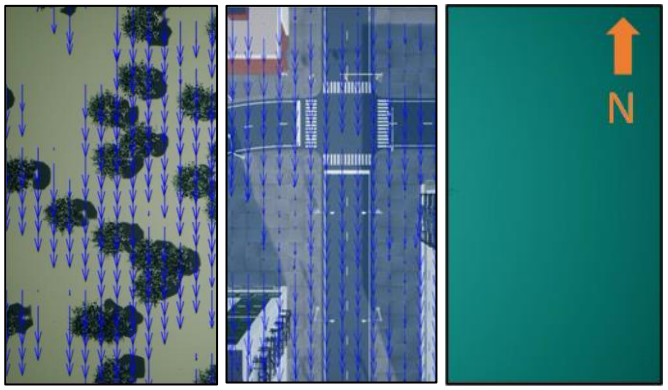

(a) (b) (c)

Figure 6. Sample of optical flow estimation for different flight scenes, (a) forest scene, (b) city block scene, and (c) water scene. The blue arrows represent optical flow vector.

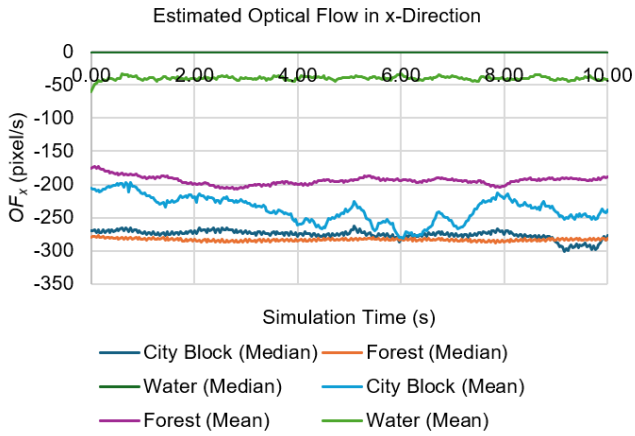

(a)

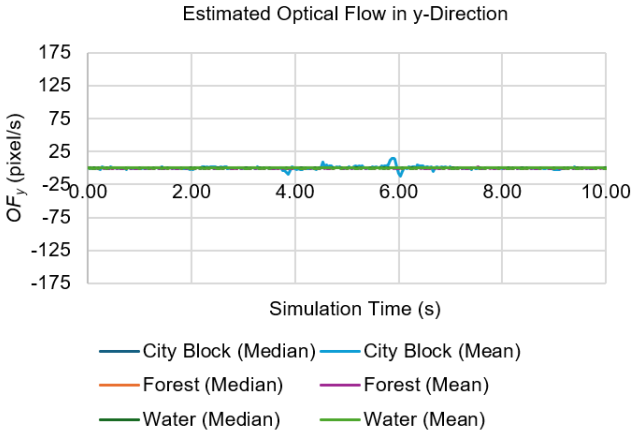

(b)

Figure 7. Global optical flow estimates for different flight scenes.

(median) and city block (median) velocity confirmed that the median value of the optical flow resulted in the best estimates with minimum mean of error (Table II). Therefore, the median value of optical flow in moderate and rich texture is better for estimating the velocity of a vehicle in a steady straight flight condition than their mean value. This finding corroborates the findings of [24], indicating that global optical flow can be derived from median value of optical flow field.

As can also be seen in Table II, the standard deviations for the mean method of global optical flow estimation are higher than median method. It can happen due to the mean method that

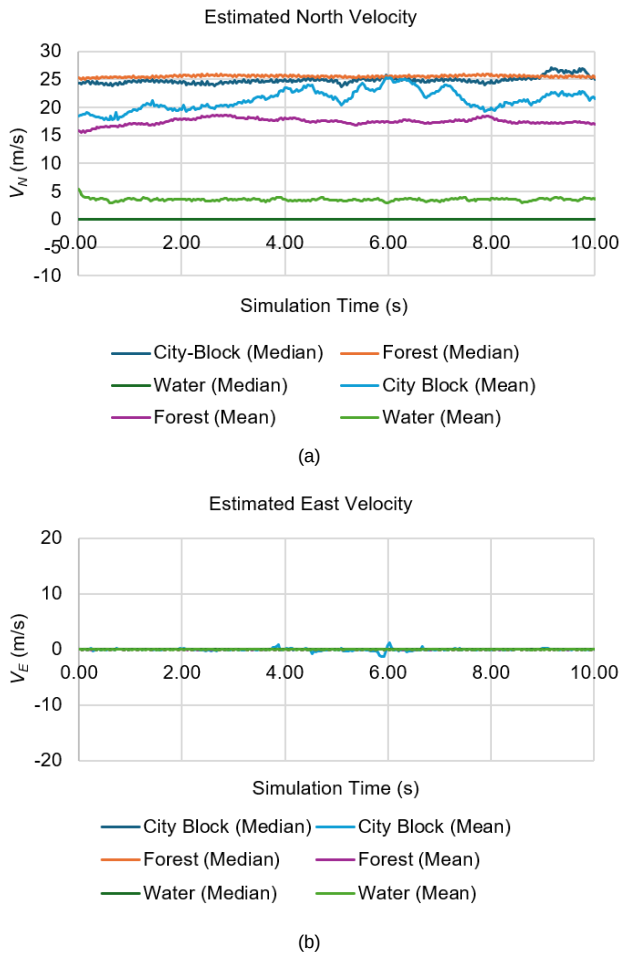

Figure 8. Graph of (a) estimated north velocity and (b) estimated east velocity for different flight scenes.

TABLE II
2D VELOCITY ESTIMATION ERROR FOR DIFFERENT FLIGHT SCENES

Scene (Method)	Mean of V_N - V_E Error (m/s)	Standard Deviation of V_N - V_E Error (m/s)
Forest (Median)	[0.6; 0]	[0.2; 0]
Forest (Mean)	[-7.3; 0]	[0.8; 0]
City-Block (Median)	[-0.3; 0]	[0.4; 0]
City-Block (Mean)	[-4.2; 0]	[1.7; 0.1]
Water (Median)	[-25; 0]	[0; 0]
Water (Mean)	[-21.5; 0]	[0.2; 0]

is more sensitive to noise in the image. As for the water scene, the optical flow estimation method could not detect the motion relative between the SUAVs and the scene. The error of the velocity estimation in water scene was up to 21.5 m/s (mean method) and 25 m/s (median method). The mean method of global optical flow yields less error because it is more sensitive to the noise. This noise appears due to the light reflection on the water surface, which can be detected by the optical flow estimation method while SUAV flights above the water surface.

B. EFFECT OF CAMERA TILT ANGLE

Three different variations of positive camera tilt angle (-10 deg, -20 deg, and 30 deg) and three different variations of negative camera tilt angle (10 deg, 20 deg, and 30 deg) were used to observe the effect of camera tilt angle. In this

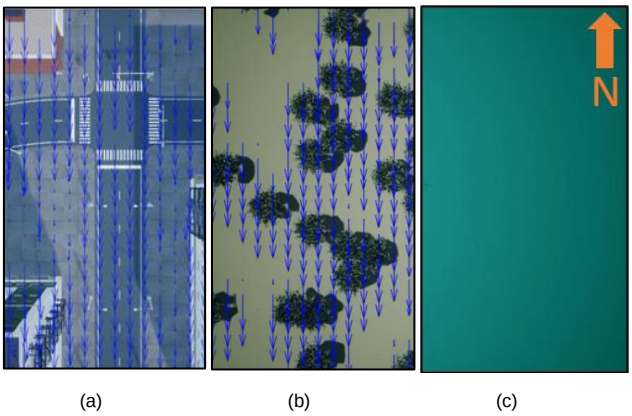

Figure 9. Sample of optical flow field for different camera tilt angle, (a) 10 deg, (b) 20 deg, (c) 30 deg. The blue arrows represent optical flow vector

observation, the median value of the optical flow was considered for velocity estimation, as shown in IV. A, the median is a better estimate for global optical flow value for steady straight flight. Figure 9 shows the example of the distribution of optical flow in the optical flow field for three different camera tilt angles, including 10 deg, 20 deg, and 30 deg. Based on Figure 9, the optical flow distribution is getting more distorted as the camera tilt angle increases. Therefore, the optical flow field distortion may contribute to the estimation errors. The distortion of the optical flow field results in the reduction of OF_x and added value in OF_y due to increased camera tilt angle. Overall, the magnitude of the optical flow in the x-direction is reduced and, in the y-direction, it is increased as the distance between the object in the scene and the camera is increased. In actual measurements, the reduction of optical flow magnitude can be considered bias from the true value.

Table III shows the mean and standard deviation of error in the estimated velocity (V_N and V_E) for each variation of camera tilt angle. Similar to the decreasing value of median optical flow in the x-direction due to increasing camera tilt angle, the estimated velocity also decreases due to this effect. As shown in Table III, for the 30-deg camera tilt angle (positive or negative), the estimated velocity for the north axis is already decreasing by more than 8 m/s. Therefore, for long periods, the bias resulting from the camera tilt angle must be corrected to obtain a good estimation of velocity and position.

C. EFFECT OF ALTITUDE

The altitude effect was observed by conducting several other simulations by slightly changing the altitude of the SUAVs in the forest scene scenario. Six variations of altitude difference (Δh) were used, including -30 m, -20 m, -10 m, 10 m, 20 m, and 30 m. Positive altitude indicates an elevation over the reference altitude (h = 100 m), whereas negative altitude means lower than 100 m. In this observation, the median value of the optical flow was considered for the velocity estimation, similar to IV. B.

Table IV shows the mean and standard deviation of errors in the estimated velocity (V_N and V_E) for each variation of the altitude difference. As shown in Table IV, as Δh (positive Δh) increases, the value of V_N reduces (negative V_N). Conversely, as Δh (negative Δh) decreases, the value of V_N increases (positive V_N). This trend aligns with expectations, given that the estimated velocity is computed from the optical flow values, which increases when the camera is closer to the ground and decreases when it is farther from the ground.

TABLE III
2D VELOCITY ESTIMATION ERROR FOR DIFFERENT CAMERA TILT ANGLE

Camera Tilt Angle (deg)	Mean of V_N - V_E Error (m/s)	Standard Deviation of V_N - V_E Error (m/s)
0	[0.6; 0]	[0.2; 0]
-10	[-1.9; 0]	[0.2; 0]
-20	[-5.5; 0]	[0.3; 0]
-30	[-9.2; 0]	[0.4; 0]
10	[-1.7; 0]	[0.2; 0]
20	[-5.2; 0]	[0.2; 0]
30	[-8.9; 0]	[0.3; 0]

TABLE IV
2D VELOCITY ESTIMATION ERROR FOR DIFFERENT ALTITUDE DIFFERENCE

Altitude Difference (m)	Mean of V_N - V_E Error (m/s)	Standard Deviation of V_N - V_E Error (m/s)
0	[0.6; 0]	[0.2; 0]
-10	[4.3; 0]	[0.2; 0]
-20	[8.2; 0]	[0.3; 0]
-30	[13.1; 0]	[0.6; 0]
10	[-1.9; 0]	[0.1; 0]
20	[-3.8; 0]	[0.1; 0]
30	[-5.4; 0]	[0.1; 0]

As seen in Table IV, the higher the altitude difference (Δh), the higher the error of the estimate. The mean of error of the velocity estimation increased significantly compared to the standard deviation of error. The increase in the mean of error indicates that the characteristic of the error due to altitude difference can be handled as bias or systematic error. Therefore, the effect of altitude difference must be considered by correcting the estimated velocity to avoid accuracy reduction by referring to (9), which relates to the optical flow and velocity estimation.

V. CONCLUSION

The result shows that optical flow can be used to estimate planar (2D) velocity in a flight scene with enough feature or texture, such as while the SUAVs fly above a city or forest. It has been shown that the optical flow estimation using the Farneback method can be used to determine the flight speed of an SUAV in steady straight flight for a specific altitude of 100 m and velocity of 25 m/s. Several conditions to consider include the texture richness of the flight scene, camera angle, and altitude. Calibration of these effects is crucial to avoid estimation bias over longer period, which can accumulate in position errors.

Future research will focus on assessing optical flow performance with various flight trajectories and testing the flight speed estimation method in real flight scenes. Furthermore, integrating optical flow with other sensors, such as IMU and GNSS, in different flight scenarios can be explored to obtain optimal SUAV navigation systems. Computing time of different optical flow algorithms and different setups can also be considered for real applications in the SUAV operation.

CONFLICTS OF INTEREST

The authors state that the research entitled "Optical Flow Performance in the SUAV Flight Speed Estimation Using Farneback Method" has no conflict of interest.

AUTHORS' CONTRIBUTIONS

Conceptualization, Aziz Fathurrahman, Yazdi Ibrahim Jenie, and Ony Arifianto; methodology, Aziz Fathurrahman; software, Aziz Fathurrahman; validation, Aziz Fathurrahman; formal analysis, Aziz Fathurrahman; investigation, Aziz Fathurrahman; writing—original draft preparation, Aziz Fathurrahman; writing—reviewing and editing, Aziz Fathurrahman; visualization, Aziz Fathurrahman; supervision, Yazdi Ibrahim Jenie, Ony Arifianto and Hari Muhammad.

REFERENCES

[1] H. Huang and A.V Savkin, "Aerial surveillance in cities: When UAVs take public transportation vehicles," IEEE Trans. Autom. Sci. Eng., vol. 20, no. 2, pp. 1069–1080, Apr. 2023, doi: 10.1109/TASE.2022.3182057.

[2] R. Kellermann, T. Biehle, and L. Fischer, "Drones for parcel and passenger transportation: A literature review," Transp. Res. Interdiscip. Perspect., vol. 4, pp. 1–13, Mar. 2020, doi: 10.1016/j.trip.2019.100088.

[3] I. Bisio et al., "A systematic review of drone based road traffic monitoring system," IEEE Access, vol. 10, pp. 101537–101555, Sep. 2022, doi: 10.1109/ACCESS.2022.3207282.

[4] M. Lyu, Y. Zhao, C. Huang, and H. Huang, "Unmanned aerial vehicles for search and rescue: A survey," Remote Sens., vol. 16, no. 13, pp. 1–35, Jul. 2023, doi: 10.3390/rs15133266.

[5] D.C. Tsouros, S. Bibi, and P.G. Sarigiannidis, "A review on UAV-based applications for precision agriculture," Information, vol. 10, no. 11, pp. 1–26, Nov. 2019, doi: 10.3390/info10110349.

[6] G. Pajares, "Overview and current status of remote sensing applications based on unmanned aerial vehicles (UAVs)," Photogramm. Eng. Remote Sens., vol. 81, no. 4, pp. 281–329, Apr. 2015, doi: 10.14358/PERS.81.4.281.

[7] T. Elmokadem and A.V. Savkin, "Towards fully autonomous UAVs: A survey," Sensors, vol. 21, no. 18, pp. 1–39, Sep. 2021, doi: 10.3390/s21186223.

[8] Y. Lu, Z. Xue, G.-S. Xia, and L. Zhang, "A survey on vision-based UAV navigation," Geo-spat. Inf. Sci., vol. 21, no. 1, pp. 21–32, Jan. 2018, doi: 10.1080/10095020.2017.1420509.

[9] X. Ye, F. Song, Z. Zhang, and Q. Zeng, "A review of small UAV navigation system based on multisource sensor fusion," IEEE Sens. J., vol. 23, no. 17, pp. 18926–18948, Sep. 2023, doi: 10.1109/JSEN.2023.3292427.

[10] D.J. Yeong, G. Velasco-Hernandez, J. Barry, and J. Walsh, "Sensor and sensor fusion technology in autonomous vehicles: A review," Sensors, vol. 21, no. 6, pp. 1–37, Mar. 2021, doi: 10.3390/s21062140.

[11] Q. Zhang, X. Niu, and C. Shi, "Impact assessment of various IMU error sources on the relative accuracy of the GNSS/INS systems," IEEE Sens. J., vol. 20, no. 9, pp. 5026–5038, May 2020, doi: 10.1109/JSEN.2020.2966379.

[12] P. Papadimitratos and A. Jovanovic, "Protection and fundamental vulnerability of GNSS," in 2008 IEEE Int. Workshop Satell. Space Commun., 2008, pp. 167–171, doi: 10.1109/IWSSC.2008.4656777.

[13] H. Chao, Y. Gu, and M. Napolitano, "A survey of optical flow techniques for robotics navigation applications," J. Intell. Robot. Syst., vol. 73, pp. 361–372, Jan. 2014, doi: 10.1007/s10846-013-9923-6.

[14] E.S. Calverts, "Visual approach and landing aids for aircraft. Fundamental problems analysed by means of perspective diagrams," R. Aircr. Establ., Farnborough, Great Britain, Report No. EL 1414, 1947.

[15] J.J. Gibson, P. Olum, and F. Rosenblatt, "Parallax and perspective during aircraft landings," Am. J. Psychol., vol. 68, no. 3, pp. 372–385, Sep. 1955, doi: 10.2307/1418521.

[16] D.C. Niehorster, "Optic flow: A history," i-Perception, vol. 12, no. 6, pp. 1–49, Nov. 2021, doi: 10.1177/20416695211055766.

[17] H.W. Ho, G. CHE de Croon, and Q. Chu, "Distance and velocity estimation using optical flow from a monocular camera," Int. J. Micro Air Veh., vol. 9, no. 3, pp. 198–208, Sep. 2017, doi: 10.1177/1756829317695566.

[18] K. McGuire et al., "Efficient optical flow and stereo vision for velocity estimation and obstacle avoidance on an autonomous pocket drone," IEEE Robot. Autom. Lett., vol. 2, no. 2, pp. 1070–1076, Apr. 2017, doi: 10.1109/LRA.2017.2658940.

[19] S.C. Diamantas and P. Dasgupta, "An active vision approach to height estimation with optical flow." in Advances in Visual Computing – ISVC 2013, 2013, pp. 160–170.

[20] O. Araar and N. Aouf, "A new hybrid approach for the visual servoing of VTOL UAVs from unknown geometries," in 22nd Mediterr. Conf. Control Autom., 2014, pp. 1425–1432, doi: 10.1109/MED.2014.6961576.

[21] N.A. Nemade and V.V Gohokar, "Comparative performance analysis of optical flow algorithms for anomaly detection," in Proc. Int. Conf. Commun. Inf. Process. (ICCIP) 2019, 2019, pp. 1–12.

[22] J.L. Barron, D.J. Fleet, and S.S. Beauchemin, "Performance of optical flow techniques," Int. J. Comput. Vis., vol. 12, no. 1, pp. 43–77, Feb. 1994, doi: 10.1007/BF01420984.

[23] I. Fantoni and G. Sanahuja, "Optic flow-based control and navigation of mini aerial vehicle," Aerosp. Lab, vol. 8, pp. 1–9, Dec. 2014, doi: 10.12762/2014.AL08-03.

[24] H. Deng et al., "Global optical flow-based estimation of velocity for multicopters using monocular vision in GPS-denied environments," Optik, vol. 219, pp. 1–14, Oct. 2020, doi: 10.1016/j.ijleo.2020.164923.